

# Modeling and simulation of materials synthesis: Chemical vapor deposition and infiltration of pyrolytic carbon

Aijun Li <sup>a</sup>, Koyo Norinaga <sup>a,b</sup>, Weigang Zhang <sup>a,c</sup>, Olaf Deutschmann <sup>a,\*</sup>

<sup>a</sup> *Intitut für Technische Chemie und Polymechemie, Universität Karlsruhe (TH), 76131 Karlsruhe, Germany*

<sup>b</sup> *Center for Advanced Research of Energy Conversion Materials, Hokkaido University, 0608628 Sapporo, Japan*

<sup>c</sup> *Institute of Process Engineering, Chinese Academy of Sciences, 100080 Beijing, China*

Received 23 March 2007; received in revised form 21 June 2007; accepted 13 July 2007

Available online 27 July 2007

## Abstract

Chemical vapor deposition and infiltration of pyrolytic carbon for the production of carbon fiber reinforced carbon is studied by modeling approaches and computational tools developed recently. Firstly, the development of a gas-phase reaction mechanism of chemical vapor deposition (CVD) of carbon from unsaturated light hydrocarbons ( $C_2H_4$ ,  $C_2H_2$ , and  $C_3H_6$ ) is presented. The mechanism consisting of 827 reactions among 227 species is based on existing information on elementary reactions and evaluated by comparison of numerically predicted and experimentally determined product compositions taking into account 44 stable gas-phase compounds formed in a tubular flow reactor. Secondly, a model and a computer code for two-dimensional transient simulations of chemical vapor infiltration (CVI) from methane into carbon fiber reinforced carbon are presented. The chemical model is based on a reduced multi-step reaction scheme for pyrolytic carbon deposition, which is derived from a mechanism based on elementary reactions, and a hydrogen inhibition model of pyrolytic carbon deposition. The coupled governing equations of mass transfer, chemical vapor deposition, surface growth, and gas-phase and surface chemical reactions are numerically solved by a finite element method (FEM). The computer code is applied to reveal densification processes of felts with fiber volume fractions of 7.1% and 14.2%. Numerically predicted bulk density distributions agree well with experimental results.

© 2007 Elsevier Ltd. All rights reserved.

**Keywords:** B. Modeling; C. Computational simulation; E. Chemical vapor deposition; E. Chemical vapor infiltration

## 1. Introduction

The numerical simulation of materials syntheses based on detailed models for the chemical kinetics and transport processes are expected to support development and optimization of production processes. Chemical reactors for materials syntheses are often characterized by interactions between chemical reactions in usually more than one phase, e.g. gas phase and solid phase, mass transport by convection and diffusion, heat transport in different phases, and the continuous variations of geometrical and physical

properties such as structure of fluid region, surface to volume ratio, and porosity.

The chemical vapor infiltration (CVI) of hydrocarbons into carbon/carbon composites has ever received a strong interest since its development in the 1960's. Although today, it is widely accepted that the interaction of homogeneous gas-phase reactions, heterogeneous surface reactions, and mass transport controls the texture and the densification mode of pyrolytic carbon (pyrocarbon), the process has not yet been understood in detail [1,2]. Isobaric and isothermal CVI of carbon is applied for the synthesis of C/C composites in the aerospace industry, e.g. rocket and missile nozzles and brake disks. A predictive and reliable model for CVI and chemical vapor deposition (CVD) of carbon is expected to accelerate the development and optimization of C/C composites.

\* Corresponding author. Tel.: +49 721 608 3138; fax: +49 721 608 4805.

E-mail addresses: [li@ict.uni-karlsruhe.de](mailto:li@ict.uni-karlsruhe.de) (A. Li), [deutschmann@ict.uni-karlsruhe.de](mailto:deutschmann@ict.uni-karlsruhe.de) (O. Deutschmann).

In this contribution, we will discuss modeling approaches for CVD and CVI processes for synthesis of carbon/carbon composites. A detailed elementary reaction mechanism for modeling of gas-phase chemistry in CVD of light hydrocarbons is proposed. A lumped surface reaction mechanism is suggested for the deposition of pyrolytic carbon from various hydrocarbon precursors. In order to simulate CVI processes, a reduced version of the gas-phase reaction model was coupled with the surface reaction mechanism and the porosity evolution model of carbon fiber felts. The model accounts for the inhibition of carbon deposition by hydrogen. Predictions of gas-phase compositions in CVD and bulk density distributions of carbon/carbon composites are compared with data derived experimentally.

## 2. Modeling approaches

### 2.1. Development of a detailed kinetic model of gas-phase reactions

In CVD and CVI of carbon, a wide variety of hydrocarbon and intermediate radicals is formed by gas-phase reactions, and all of these species have a potential to chemisorb or physisorb on the growing pyrolytic carbon surface and, thus, to be integrated into the structure of pyrolytic carbon. A gas-phase reaction model was developed to simulate gas-phase reactions in CVD of carbon from unsaturated light hydrocarbons by compiling elementary reaction models reported in the literature. The reaction mechanism developed consists of 227 species in 827 reactions. The development of the reaction mechanism is based on the following approach:

First, hydrocarbon reactions are extracted from the mechanism for the formation of aromatics in acetylene and ethylene flames reported by Wang and Frenklach [3]. This mechanism is very comprehensive and covers the formation of polycyclic aromatic hydrocarbons up to pyrene but does not include the formation of hydrocarbons with odd numbers of carbon atoms such as toluene and indene. These latter reaction pathways were supplemented by a mechanism developed by Marinov et al. [4]. The detailed reactions on the C<sub>3</sub>- and C<sub>4</sub>- species are included from the mechanism reported by Hidaka et al. [5] and Tsang [6]. The formation mechanisms proposed by Richter and Howard [7] for the larger polycyclic aromatic hydrocarbons (PAH) up to coronene were added to account for those larger species experimentally detected in the gas-phase composition.

The model is validated by comparison of the computational with experimental results for homogeneous gas-phase pyrolysis of ethylene, acetylene, and propylene as well as for heterogeneous CVD of pyrocarbon from those precursors [8,9]. Concentrations of 44 species including hydrogen and hydrocarbons ranging from methane to coronene are analyzed. Sensitivity analyzes identifying elementary reactions with major influence on the overall process supports the development of the mechanism.

More details of the mechanism development can be found in our previous papers [8,9]; the mechanism can be downloaded [10].

### 2.1.1. Multi-step chemical vapor deposition and hydrogen inhibition model of pyrocarbon

Modeling and simulation of CVI are much more complicated than those of CVD, because the model needs to account for the dynamically evolving porous structures in CVI. Due to computational costs, it is impractical (CPU) to simulate CVI processes treating all gas-phase species as pyrocarbon precursors, though all stable and intermediate species, in particular radicals, can potentially form pyrolytic carbon on solid surfaces. Furthermore, in the present work methane is used as carbon precursor and the mechanism of methane pyrolysis is considerably less understood in the temperature regime of CVD/CVI than those of C<sub>2</sub>-pyrolysis [11–16], which were mainly applied in the validation of the above described mechanisms of elementary reactions [8,9]. Thus lumped gas-phase and surface reaction mechanism were developed to calculate carbon deposition from those gas-phase species that dominate CVI of pyrolytic carbon from methane.

A qualitative picture of the complex reaction mechanism of CVD of pyrolytic carbon from light hydrocarbons was proposed by Hüttinger [17]. In the present work, we couple a multi-step chemical vapor deposition model with a heterogeneous surface reaction model of hydrogen inhibition of carbon deposition. The principles reaction pathways are shown in Fig. 1. A reduced gas-phase consecutive reaction mechanism is employed to calculate overall gas-phase reaction kinetic data ( $k_1$ – $k_4$ ) [18]. Original surface reaction kinetic data ( $k_6$ – $k_8$ ) are obtained by fitting them to CVD experimental results [19–21]. Based on the hydrogen inhibition model proposed before [22], effective surface reaction kinetic data  $K_i$  ( $i = 6, 7, 8$ ) of CVI are defined as  $k_i f_i$ , where  $f_i$  is the hydrogen inhibition function. All surface reaction kinetic data used in the present work are listed in Table 1. Carbon deposition from methane directly is not likely to proceed and, therefore, neglected in the current model.

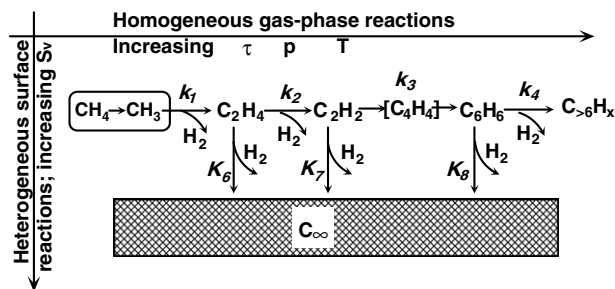


Fig. 1. Multi-step chemical vapor deposition and hydrogen inhibition of pyrocarbon from methane ( $\tau$  the residence time,  $p$  the pressure,  $T$  the temperature,  $S_v$  volume-related surface area).

Table 1  
Original surface reaction kinetic data of various species

Species	Surface reaction kinetic data (in Arrhenius format)			
	$A$ (m/s)	$E_A$ (kJ/mol)	$k_{1368K}$ (m/s)	Hydrogen inhibition function $f_i$
$C_2H_4$	$7.24E+01$	155.0	$8.74E-05$	$1.104 / \left(1.104 + \frac{[H_2]}{[C_2H_4]}\right)$
$C_2H_2$	$1.35E+01$	126.0	$2.09E-04$	$3.269 / \left(3.269 + \frac{[H_2]}{[C_2H_2]}\right)$
$C_6H_6$	$4.71E+05$	217.0	$2.44E-03$	$0.5887 / \left(0.5887 + \frac{[H_2]}{[C_6H_6]}\right)$

### 2.1.2. Mass transfer model and pore structure evolution model

The major differences of CVI in comparison to CVD are the large surface area of the CVI substrate and the continuous variation of the surface area due to progressive densification of the porous substrates, which dramatically influence the interactions of gas-phase and surface kinetics. In the present work, a surface area model for carbon felts with randomly distributed, non-overlapping fibers is employed. The evolution of the volume-related surface area as well as the equivalent radius of pores is calculated numerically. Fig. 2 shows the evolution of the porous structure as a function of porosity.

The CVI reactor and its geometrical model used in the present work were described in detail before [22,23]. Generally, the reactor can be divided into two parts: the free flow sub-domain (the narrow gap from the inlet to the outlet) and the porous sub-domain (the felt). Obviously, the model for the processes in the free flow sub-domain needs to include diffusion, convection, and chemical reactions. Surface reactions in this sub-domain can be neglected because the very small surface area does not significantly affect the gas-phase composition. On the other side, mass transfer by convection inside the felt can be neglected [24]. The two-dimensional (2D) transient mass transfer equations coupled with evolution equations of porosity and bulk density

and the chemical source terms are solved to simulate CVI of the carbon fiber felts [22].

### 2.1.3. Simulation platforms

Simulations of gas-phase reactions in CVD were conducted using two computational tools, DETCHEM<sup>PLUG</sup> [10] for simulation of a plug flow reactor with axial temperature profile and HOMREA [25] for simulation of a homogeneous reaction system and sensitivity analysis. The input data include the physical model parameters such as forward reaction rate expressions and thermodynamic polynomials for all participating species, as well as the operating conditions such as temperature, pressure, inlet velocity, and the mixture concentration at the inlet.

The present CVI model was numerically implemented by coupling COMSOL for FE (finite element) simulation with MATLAB for post-processing. Corresponding to the experimental setup, densification of carbon felts with initial fiber volume fractions of 7.1% and 14.2% were simulated. The carbon fiber felt with an initial fiber volume fraction of 14.2% is obtained by pressing the carbon felt of 7.1%. Other process parameters used for CVI simulation are the temperature (1368 K), the methane pressure (22.5 kPa) at the inlet and the inlet flow velocity ( $0.45 \text{ m s}^{-1}$ ).

## 3. Results and discussion

### 3.1. Simulation of gas-phase composition in CVD of carbon

Fig. 3 shows the measured and predicted mole fractions of major chemical components found at the exit of the CVD reactor operated at a furnace temperature of 900 °C and a pressure of 15 kPa using ethylene (a), acetylene (b) and propylene (c) as precursors. For details of the experimental procedure it is referred to Refs. [8,9]. The mole fractions are plotted as a function of the effective

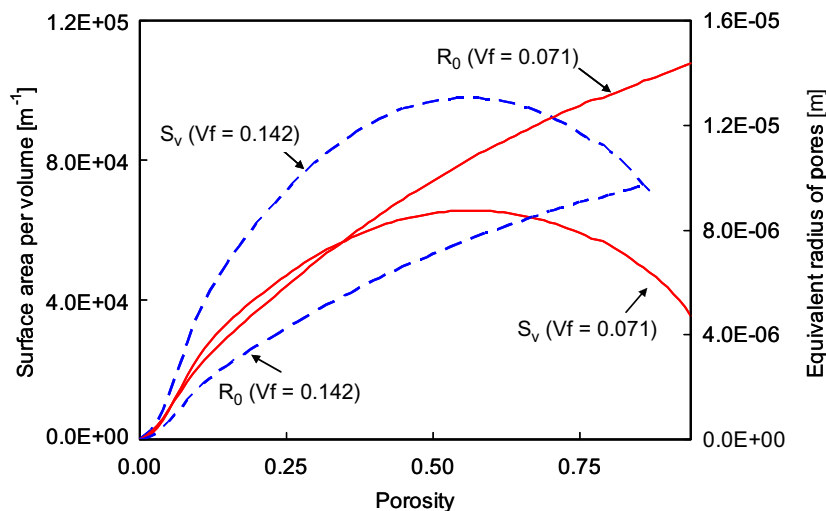


Fig. 2. Evolutions of equivalent radius ( $R_0$ ) of pores and volume-related surface area ( $S_v$ ) for carbon fiber felts as a function of porosity.

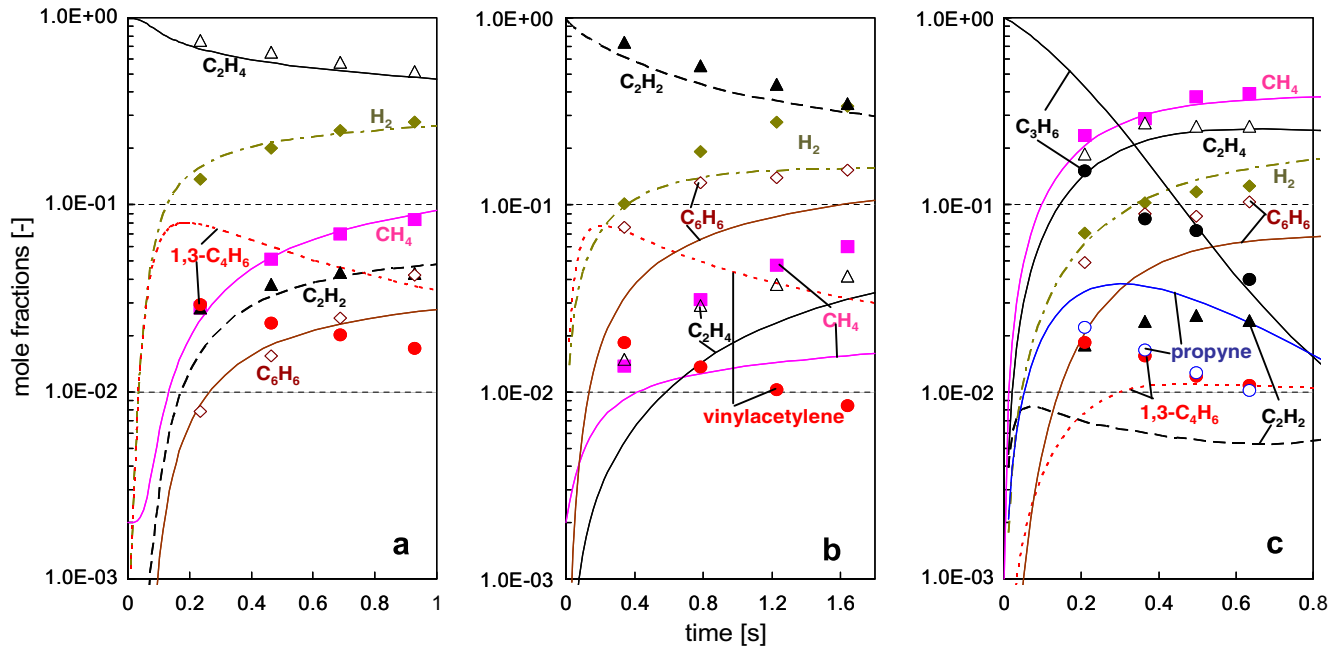


Fig. 3. Comparison of model predictions (lines) with experimental mole fraction profiles (symbols) of major species during pyrolysis of ethylene (a), acetylene (b), and propylene (c) in a flow reactor at 900 °C and 15 kPa.

residence time at the isothermal zone in the reactor. In ethylene pyrolysis (Fig. 3a), the model very well predicts the consumption of ethylene as well as the formation of hydrogen, methane, acetylene, and benzene, while the formation of 1,3-butadiene is over-predicted. Nevertheless, the prediction curves well reproduce the experimentally observed trends for all species, also the ones not shown but observed experimentally. As shown in Fig. 3b, the consumption of acetylene and the product formation are also fairly well predicted. A significant over-prediction is observed for vinylacetylene. The prediction curves reproduce the experimentally observed trends for all other species. In case of propylene as precursor (Fig. 3c), the consumption of propylene is under predicted at residence times less than 0.5 s, but it is well predicted at longer residence times. Methane, ethylene, and hydrogen profiles are well reproduced by the model. The curves representing the simulation results also capture the experimental trends except for acetylene and 1,3-butadiene.

### 3.2. Simulation of bulk density and surface-related deposition rate

The bulk density of carbon/carbon composites is the most attractive and also an easily measured parameter. For most applications a key goal is the achievement of a high and uniform bulk density in a short densification time. Fig. 4 compares the experimentally measured (symbols) and simulated (lines) profiles of the bulk density as a function of the infiltration time. As expected, the increasing initial fiber volume fraction (Vf) leads to a higher bulk density for short densification times, the mass gain after the first 60

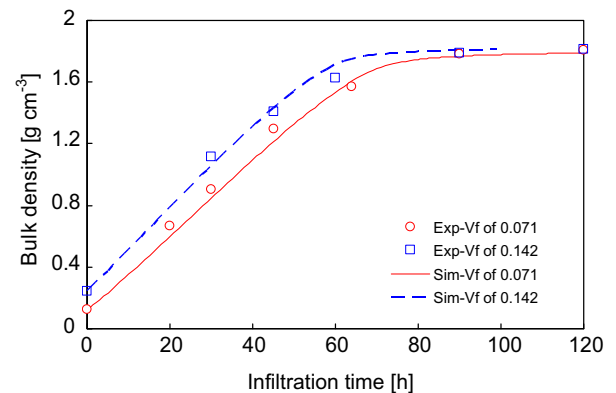


Fig. 4. Densification profiles of felts with various fiber volume fractions (Vf) as a function of the infiltration time. Symbols: experimental results; lines: simulation results.

hours, however, is very similar. According to the model shown in Fig. 1, the volume-related deposition rate,  $R_C$ , is defined as:

$$R_C = S_v(K_6 \cdot [C_2H_4] + K_7 \cdot [C_2H_2] + K_8 \cdot [C_6H_6])$$

Where  $S_v$  defines the surface area to volume ratio of carbon fiber felts and  $[X]$  denote the concentrations of species X. Obviously, an increase of  $S_v$  does not necessarily lead to an increase of  $R_C$ , because increasing  $S_v$  indirectly hinders mass transfer inside the porous medium leading to a decrease of  $(K_6 \cdot [C_2H_4] + K_7 \cdot [C_2H_2] + K_8 \cdot [C_6H_6])$ , which is the surface-related deposition rate. In fact, the result of the simulation confirms this consideration. As shown in Fig. 5, the average surface-related deposition rate for the felt with the larger initial fiber fraction is always smaller

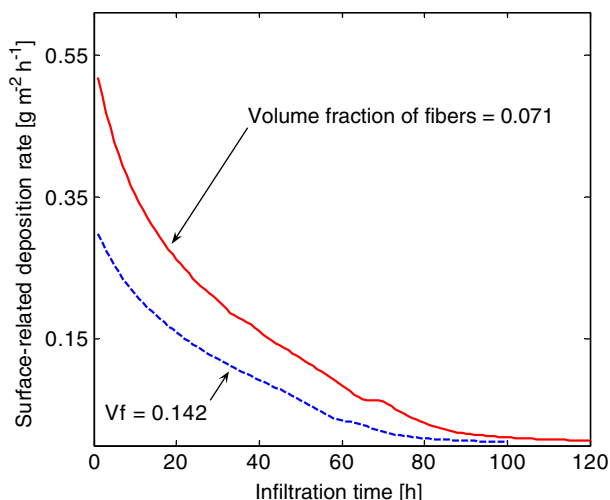


Fig. 5. Average surface-related deposition rate of pyrocarbon as a function of the infiltration time. Solid line: Initial fiber volume fraction = 7.1%; dashed line: 14.2%.

than that for the felt with the lower one. The behavior also suggests a shift of the gas-phase composition from aromatic species to small linear species for increasing  $S_v$ . Subsequently, the overall surface-deposition rate will decrease dramatically. Moreover, due to the relative increase of linear species exhibiting a considerably higher diffusivity than aromatic species, the filling efficiency of micropores will be enhanced, resulting in a decreasing volume fraction of closed pores. The above deduction is qualitative, but con-

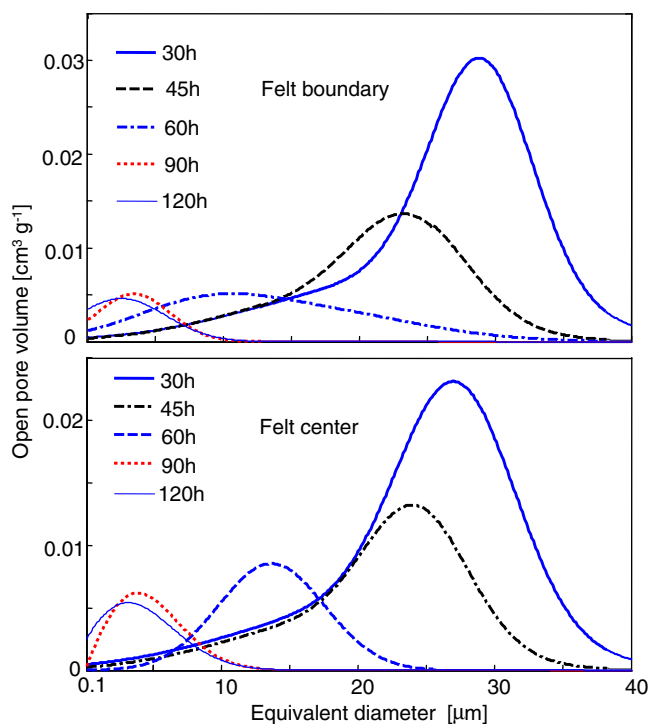


Fig. 6. Distribution of the open porosity as a function of the equivalent diameter of open pores for the carbon felt with the initial fiber volume fraction of 0.142.

sistent. In Fig. 6, the measured distribution of the volume of open pores is shown as a function of the equivalent diameter of the open (void) pores. The height of the maxima as well as the width of the pore size distribution decreases with increasing densification time. Furthermore the volume of the open pores at the boundary of the felt significantly exceeds the volume of the open pores in the center of the felt, which is understood by a larger ratio of aromatic to linear species in the center.

### 3.3. Simulation of bulk density distribution

Successful densification from the center to the boundary region of the porous substrates frequently is a major request of the materials synthesis process. CVI was always regarded as a diffusion-limited process, and, therefore, the CVI reactors are commonly operated at low infiltration rates and low pressure [26,27]. Recently, the densification from the center to the boundary was achieved [23,28]. Simulation results shown in Fig. 7 confirm the experimentally derived conclusions leading to the process illustration given in Fig. 1. As shown in Fig. 2, the maximum of  $R_o$  is at the beginning of the densification process; however  $S_v$  reaches its maximum at decreased porosity, i.e. much later. These facts are explained by the diffusion of small hydrocarbon species into the porous substrate and of hydrogen outward the substrate. Hence the concentration of aromatic species and carbon deposition rate will increase in the center. At progressed densification,  $S_v$  reaches a maximum and then decreases again while  $R_o$  decreases continuously. This behavior has severe consequences on the gas-phase composition in pores. Furthermore, the bulk density distribution strongly varies from the bottom to the top of the carbon felt, i.e. in flow direction, during the last stage of densification.

It should also be pointed out that the computed density gradient of the surface region from the top to the bottom exceeds that of experiments, while the computed density gradients from the center to the boundary region are smaller than the experimentally determined gradients. These findings can be attributed to the simplified reaction model used here, which is not able to accurately predict gas-phase composition.

### 3.4. Consumption of the aromatic and linear species

Although it is not yet known how the gas-phase composition affects textures of pyrolytic carbon, it is clear that small linear species have different effects on carbon texture than aromatic species. Lieberman and Pierson [29] established a CVD model for carbon deposition correlating pyrocarbon density to the  $[C_2H_n]/[C_6H_m]$  ratio. Fig. 8 displays the spatial distribution of bulk density and consumption ratio of aromatic to linear species after one hour densification. Apparently the consumption ratio can be associated to the bulk density distribution of C/C composites. This also suggests that texture variations of pyrolytic

Experimental results of the carbon felt ( $V_f = 0.071$ ), corresponding computed results

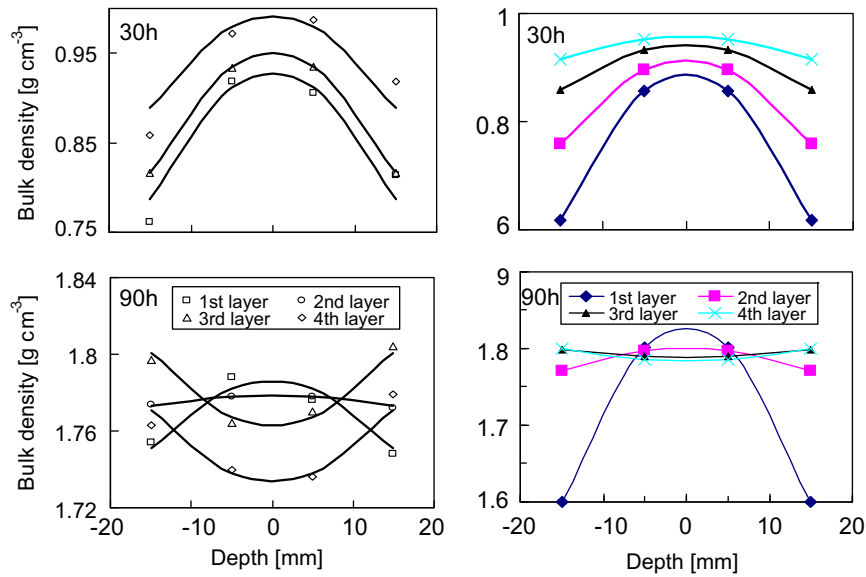


Fig. 7. Comparison between experimentally determined and simulated density distribution (the sample was divided into four layers from its bottom to the top; the first layer is the lowest part).

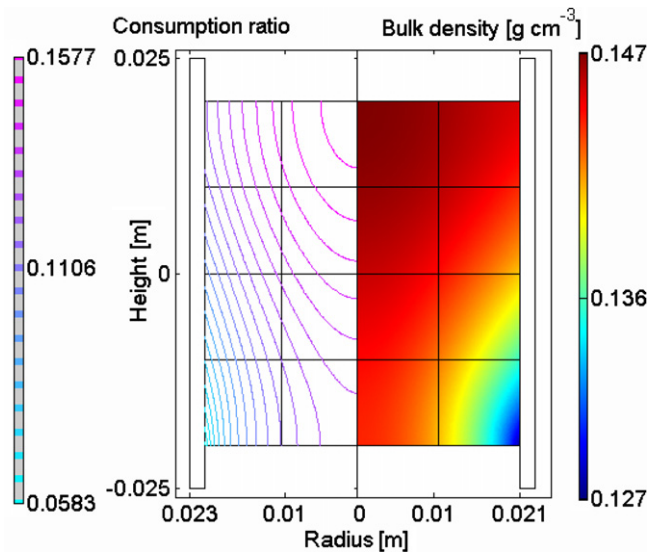


Fig. 8. Simulated distribution of density and contour of C6 over C2 consumption ratio after 1 h densification of the felt with 7.1% fiber volume fraction.

carbon may result from that varying consumption ratio of aromatic to linear species caused by the evolution of the porosity.

### 3.5. Methane consumption and carbon yield

Residual fraction of methane (one minus methane conversion) inside the reactor as predicted by the model is shown in Fig. 9. Obviously, an increasing initial fiber volume fraction does not strongly affect the consumption of

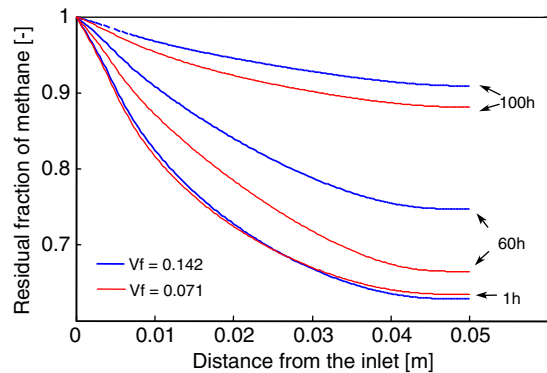


Fig. 9. Computed residual fraction of methane after 1 h, 60 h and 100 h densification.

methane, supporting the assumption that methane does not immediately contribute to the formation of deposits on the surface of the substrate. With increasing infiltration time, however, methane consumption is inhibited dramatically, indicating that the variation of the properties of the fiber felt during densification and the gas-phase species concentrations have a strong effect on methane pyrolysis. According to the multi-step chemical vapor deposition and hydrogen inhibition model, it is clear that the decomposition of methane only depends on gas-phase reaction kinetics. Higher methane consumption at the beginning of CVI means a longer effective residence time of methane inside the felts, because of complex open pore structures. However, more and more closed pores lead to very short residence times and thus lower methane consumption at the end of CVI processes. In order to investigate the effects of increasing fiber volume fractions on carbon deposition,

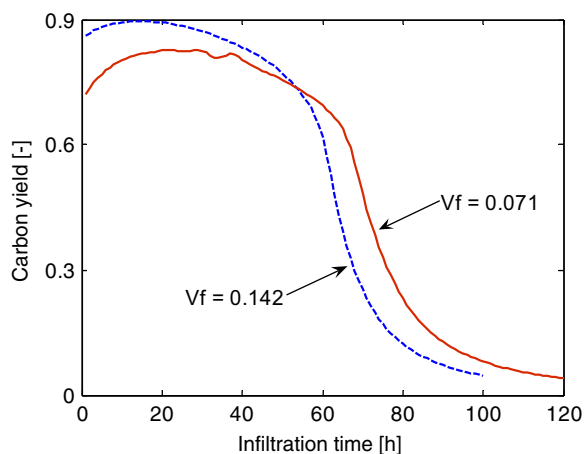


Fig. 10. Computed carbon yield as a function of infiltration time (related to methane conversion and carbon selectivity).

the yield of carbon is given in Fig. 10, which is defined as the carbon-related selectivity of the amount of carbon deposited scaled by the total amount of methane converted and entering the felt. It is clear that the carbon yield is higher at the beginning of the CVI process and is lower once the process is dominated by mass transfer. A higher initial fiber volume fraction will result in a higher carbon yield. Then, however, a more rapid decrease of carbon yield with infiltration time is observed for the felt with the higher initial fiber volume fraction. As shown in Fig. 10, the carbon yield of 90% predicted for a felt exhibiting a fiber fraction of 14.2% suggests that carbon fiber felts work as a “Starve Reactor” and a further increase of the fiber volume fraction may lead to only a slightly increase of carbon yield.

#### 4. Summary

We presented an approach for coupling gas-phase reactions and surface reactions to investigate chemical vapor infiltration for the production of carbon/carbon composites. The gas-phase composition in CVD of carbon from ethylene, acetylene, and propylene is calculated based on an elementary reaction mechanism consisting of 227 species and 827 reactions. Experimental data obtained from a conventional flow reactor are used for model validation. Satisfying agreements are found between the computations and the experimental results for major hydrocarbon species.

An inside–outside densification mode was confirmed by numerical simulations of CVI processes. An increasing initial fiber volume will result in a decreasing surface-related deposition rate but also in an increasing efficiency of filling the micropores. The predicted methane consumption implies that the decomposition of methane mainly depends on the kinetics of gas-phase reactions. Moreover, the predicted carbon yields during the early stage of the CVI process show that, as a starve reactor, the carbon fiber felts can absorb almost all carbon from methane infiltrated into the felts.

#### Acknowledgements

We thank K.J. Hüttinger for discussions on the hydrogen inhibition model and thank A. Pfrang and T. Schimmel for providing their simulation results concerning the pore model. The research was performed in the Sonderforschungsbereich 551 “Carbon from the gas-phase: elementary reactions, structures, materials”, financially supported by the Deutsche Forschungsgemeinschaft.

#### References

- [1] Savage G. Carbon–carbon composites. London: Chapman & Hall; 1992.
- [2] Fitzer E, Manocha L. In: Carbon reinforcements and carbon/carbon composites. Berlin, Heidelberg: Springer; 1998.
- [3] Wang H, Frenklach MA. A detailed kinetic modeling study of aromatics formation in laminar premixed acetylene and ethylene flames. *Combust Flame* 1997;110:173–221.
- [4] Marinov NM, Pitz WJ, Westbrook CK, Castaldi MJ, Senkan SM. Modeling of aromatic and polycyclic aromatic hydrocarbon formation in premixed methane and ethane flames. *Combust Sci Technol* 1996;116:211–87.
- [5] Hidaka Y, Higashihara T, Ninomiya N, Masaoka H, Nakamura T, Kawano H. Shock tube and modeling study of 1,3-butadiene pyrolysis. *Int J Chem Kinet* 1996;28:137–51.
- [6] Tsang W. Chemical Kinetic Data-Base for Combustion Chemistry. 5. Propene. *J Phys Chem Ref Data* 1991;20:221–73.
- [7] Richter H, Howard JB. Formation and consumption of single-ring aromatic hydrocarbons and their precursors in premixed acetylene, ethylene and benzene flames. *Phys Chem Chem Phys* 2002;4: 2038–55.
- [8] Norinaga K, Deutschmann O. Detailed gas-phase chemistry in CVD of carbon from unsaturated light hydrocarbons. In: Proc. of 15th European conference on chemical vapor deposition. Electrochemical society proceeding volume 2005;9:348–55.
- [9] Norinaga K, Deutschmann O. Detailed kinetic modeling of gas-phase reactions in the chemical vapor deposition of carbon from light hydrocarbons. *Ind Eng Chem Res* 2007;46(11):3547–57.
- [10] Deutschmann O, Tischer S, Correa C, Chatterjee D, Kleditzsch S, Janardhanan VM, Mladenov N. DETCHEM software package. 2.1 ed. <www.detchem.com>, Karlsruhe; 2006.
- [11] Dean AM. Detailed kinetic modeling of autocatalysis in methane pyrolysis. *J Phys Chem* 1990;94:1432–9.
- [12] Matheu DM, Dean AM, Grenda JM, Green WH. Mechanism generation with integrated pressure dependence: a new model for methane pyrolysis. *J Phys Chem* 2003;107:8552–65.
- [13] Grenda JM, Androulakis IP, Dean AM. Application of computational kinetics mechanism generation to model the autocatalytic pyrolysis of methane. *Ind Eng Chem Res* 2003;42:1000–10.
- [14] Glasier GF, Pacey PD. Formation of porous carbon during the pyrolysis of ethane at high conversions. *Carbon* 2001;39:15–23.
- [15] Matheu DM, Grenda JM. A systematically generated, pressure-dependent mechanism for high-conversion ethane pyrolysis. 1. Pathways to the minor products. *J Phys Chem* 2005;109:5332–42.
- [16] Matheu DM, Grenda JM. A systematically generated, pressure-dependent mechanism for high-conversion ethane pyrolysis. 2. Radical disproportionations, Missing families, and the consequences of pressure dependence. *J Phys Chem* 2005;109:5343–51.
- [17] Hüttinger KJ. CVD in hot wall reactors – the interaction between homogeneous gas-phase and heterogeneous surface reactions. *Adv Mater-CVD* 1998;4(4):151–8.
- [18] Li HJ, Li AJ, Bai RC, Li KZ. Numerical simulation of chemical vapor infiltration of propylene into C/C composites with reduced multi-step kinetic models. *Carbon* 2005;43:2937–50.

- [19] Becker A, Hu ZJ, Hüttinger KJ. A hydrogen inhibition model of deposition from hydrocarbon. *Fuel* 2000;79:1573–80.
- [20] Becker A, Hüttinger KJ. Chemistry and kinetics of chemical vapor deposition of pyrocarbon—III pyrocarbon deposition from propylene and benzene in the low temperature regime. *Carbon* 1998;36(3):201–11.
- [21] Becker A, Hüttinger KJ. Chemistry and kinetics of chemical vapor deposition of pyrocarbon—II pyrocarbon deposition from ethylene, acetylene and 1,3-butadiene in the low temperature regime. *Carbon* 1998;36(3):177–99.
- [22] Li AJ, Deutschmann O. Transient modeling of chemical vapor infiltration of methane using multi-step reaction and deposition models. *Chem Eng Sci*, in press, doi:10.1016/j.ces.2007.01.069.
- [23] Zhang WG, Hüttinger KJ. Chemical vapor infiltration of carbon fiber felt: optimization of densification and carbon microstructure. *Carbon* 2002;40(14):2529–45.
- [24] Leutard D, Vignoles GL, Lamouroux F, Bernard B. Monitoring density and temperature in C/C composites processing by CVI with induction heating. *J Mater Synth Proces* 2002;9(5):259–83.
- [25] Warnatz J, Maas U, Dibble RW. *Combustion*. Springer-Verlag: Heidelberg, New York; 2000.
- [26] Kotlenski WV. Deposition of pyrolytic carbon in porous solids. In: Walker Jr PL, Thrower PA, editors. *Chemistry and physics of carbon*, vol. 9. New York: Marcel Dekker; 1973. p. 173–262.
- [27] Golecki I. Recent advances in rapid densification of thick refractory by inductively heated, thermal gradient, flowing gas, isobaric chemical vapor infiltration. In: Allendorf MD, Bernard C, editors. *Proceedings of the 14th international conference of EuroCVD-11*. Paris: Electrochemical Society; 1997. p. 568–75.
- [28] Zhang WG, Hüttinger KJ. Simulation studies on chemical vapor infiltration of carbon. *Compos Sci Technol* 2002(62):1947–55.
- [29] Pierson HO, Lieberman ML. The chemical vapor deposition of carbon on carbon fibers. *Carbon* 1975;13:159–66.